Inorganic Chemistry

Article

pubs.acs.org/IC

Structure and Magnetism in Fe–Gd Based Dinuclear and Chain Systems. The Interplay of Weak Exchange Coupling and Zero Field Splitting Effects

Marilena Ferbinteanu,*[,†] Fanica Cimpoesu,*[,‡] Mihai A. Gîrţu,[§] Cristian Enachescu,[∥] and Stefania Tanase[⊥]

[†]University of Bucharest, Faculty of Chemistry, Inorganic Chemistry Department, Dumbrava Rosie 23, Bucharest 020462, Romania

[‡]Institute of Physical Chemistry, Splaiul Independentei 202, Bucharest 060021, Romania

[§]Ovidius University of Constanţa, Department of Physics, Constanţa 900527, Romania

[∥]"A. I. Cuza" University, Department of Physics, Iasi 700506, Romania

[⊥]Van't Hoff Institute of Molecular Sciences, University of Amsterdam, Science Park 904, 1098 XH Amsterdam, The Netherlands

Supporting Information

ABSTRACT: The synthesis and characterization of two Fe–Gd systems based on bpca$^-$ (Hbpca = bis(2-pyridilcarbonyl)amine) as bridging ligand is presented, taking the systems as a case study for structure–property correlations. Compound **1**, $[Fe_{LS}^{II}(\mu\text{-bpca})_2Gd(NO_3)_2(H_2O)]NO_3{\cdot}2CH_3NO_2$, is a zigzag polymer, incorporating the diamagnetic low spin Fe_{LS}(II) ion. The magnetism of **1** is entirely determined by the weak zero field splitting (ZFS) effect on the Gd(III) ion. Compound **2** is a Fe(III)–Gd(III) dinuclear compound, $[Fe_{LS}^{III}(bpca)(\mu\text{-bpca})Gd(NO_3)_4]{\cdot}4CH_3NO_2{\cdot}CH_3OH$, its magnetism being interpreted as due to the antiferromagnetic coupling between the $S_{Fe} = {}^1/_2$ and $S_{Gd} = {}^7/_2$ spins, interplayed with the local ZFS on the lanthanide center. In both systems, the d–f assembly is determined by the bridging capabilities of the ambidentate bpca$^-$ ligand, which binds the d ion by a tridentate moiety with nitrogen donors and the f center by the diketonate side. We propose a spin delocalization and polarization mechanism that rationalizes the factors leading to the antiferromagnetic d–f coupling. Although conceived for compound **2**, the scheme can be proposed as a general mechanism. The rationalization of the weak ZFS effects on Gd(III) by multiconfiguration and spin–orbit *ab initio* calculations allowed us to determine the details of the small but still significant anisotropy of Gd(III) ion in the coordination sites of compounds **1** and **2.** The outlined methodologies and generalized conclusions shed new light on the field of gadolinium coordination magnetochemistry.

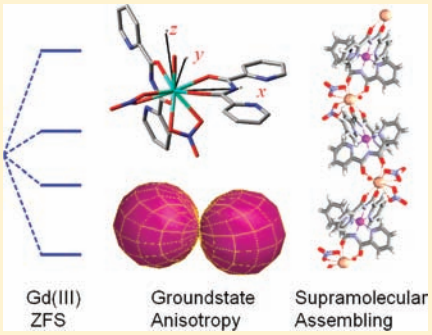

1. INTRODUCTION

A great deal of attention is currently being paid to the chemical properties of the lanthanide molecular compounds. This is because of their use in magnetic[1] and optical devices, as well as their utility as luminescence probes[2] and catalytic materials.[3] The behavior of lanthanide molecular compounds in solution is also important. Especially, the gadolinium(III) compounds have been found to be useful as contrast agents for magnetic resonance imaging (MRI)[4] based on the dynamic aspects of their magnetism.

With respect to the molecular magnetism of lanthanide ions,[5,6] the gadolinium(III) complexes are regarded as the simplest congeners in the series. This is due to the nondegenerate orbital state and the spin-only nature of the magnetism. However, Gd(III) can offer occasion for further insight and surprises. The ion can carry a small anisotropy, in the form of a zero field splitting (ZFS) effect, which, though small, can drive the low temperature magnetic behavior or enter in competition with weak exchange effects.[7] Such a situation will be presented in the following, by detailed analysis of systems containing the Gd(III) ion. We combine an experimental approach with a theoretical analysis of the situations when the ZFS alone or the interplayed ZFS and exchange coupling can shape the magnetic behavior of the homo- and heteronuclear complexes containing gadolinium(III).

The analysis of relatively small ZFS effects on Gd(III) sites exceeds the simple academic interest, because of an important application of the dynamics driven by such effects in magnetic resonance imaging (MRI).[4] The biochemical, EPR, and kinetic aspects[8] are beyond our actual focus, but any rationalization achieved in these causal factors has an important potential impact in the application field.

The anionic ligand abbreviated bpca$^-$ (Hbpca = bis(2-pyridylcarbonyl)amine) is particularly suited for assembling d–f systems. It was previously used for the synthesis of oligo-and polynuclear systems made of homo- and heterometallic d-transition metal ions.[9] Recently, we observed and exploited[10,11] the propensity of this ligand to build d–f systems, due to the natural affinities of the ions for the two donor sets, with the

Received: November 21, 2010
Published: December 9, 2011

 © 2011 American Chemical Society dx.doi.org/10.1021/ic1023289 | *Inorg. Chem.* 2012, 51, 40–50

nitrogen donors oriented toward the transition metal sites and the diketonate chelatic moiety binding to the oxophilic lanthanide ions.

We report here case studies performed on $[Fe_{LS}^{II}(\mu\text{-bpca})_2\text{-}Gd(NO_3)_2(H_2O)]NO_3\cdot 2CH_3NO_2$ (**1**), as a system for which the magnetism is driven solely by the ZFS effect on gadolinium, and the congener, $[Fe_{LS}^{III}(bpca)(\mu\text{-bpca})Gd(NO_3)_4]\cdot 4CH_3NO_2\cdot CH_3OH$ (**2**), as a compound for which Heisenberg exchange coupling and the local anisotropy are competing.

The analysis of compound **1** revealed important details of the considered system and general methodological advances regarding the characterization of the small anisotropy due to the weak ZFS manifestations on Gd(III) sites. Compound **2** showed antiferromagnetic coupling, suggested also by *ab initio* calculations. The results were extrapolated, pointing to a general mechanism for the case of the antiferromagnetic interaction in the transition metal−lanthanide complexes. This question is a counterpart to the previously clarified paradigm for the mechanism of ferromagnetic coupling,[12] raised for the situation of quasi-generalized ferromagnetism in Cu−Gd complexes.[13,14]

The key feature of the ferromagnetic mechanism is the delocalized spin density from the 3d-metal ion, via the bridging ligand, toward the 5d empty AOs of the embedded lanthanide ion. The chemical bonding of the lanthanide is practically realized by the help of its virtual 5d and 6s AOs, without implication of the f paramagnetic shell.[15] The percolation of a residual spin density into the 5d AOs is a natural fact accompanying the d−f association. At the same time, the unpaired electrons on orthogonal orbitals of the same atom tend to keep their spins in mutual parallel arrangement. As a consequence, the $\delta\alpha$ spin density, created by the main 3d α-spin carrier, induces the α-parallel orientation of the spins in the f shell. According to this general mechanism, the ferromagnetism of the d−f coupling seems favored in a rather large number of circumstances, beyond the celebrated Cu−Gd encounters. In this perspective, the clarification of an alternate mechanism, responsible for the antiferromagnetic d−f situations, is an important contribution to an open question.

The characterization of considered systems was completed with the help of *ab initio* techniques. Here, we must point out that there is a consensus that the treatment of lanthanide systems is not a routine task.[16] The methodology was designed earlier, with the first *ab initio* calculations of d−f systems being reported by us in 2004.[12]

The difficulties reside in severe convergence problems, determined by the non-*aufbau* nature of the f shell. These problems were solved by us by avoiding the usual single determinant preliminary steps, customarily used to prepare molecular orbitals entering in the multiconfiguration techniques. In turn, we enter directly in the multiconfiguration approach with orbitals preliminarily prepared by the corresponding merging of fragment wave functions (such as the d metal ion complexes plus free lanthanide ion, plus the ligands of the lanthanide coordination sphere). Several other *ab initio* multiconfiguration calculations appeared for lanthanide systems,[17] *a posteriori* to our methodological outlining.[18] Other authors[16] used density functional theory broken symmetry calculations on prototypic Cu−Gd systems, acknowledging also the intrinsic difficulties related to the non-*aufbau* issues.

2. EXPERIMENTAL AND COMPUTATION DETAILS

2.1. Materials. All chemicals and solvents were used as received, and no purification was needed. $[Fe(bpca)_2]\cdot H_2O$ and $[Fe(bpca)_2]NO_3$ were synthesized as described elsewhere.[19]

2.2. Syntheses. Compound **1** was obtained by adding a solution of $Gd(NO_3)_3\cdot 6H_2O$ (0.05 mmol) in methanol (2 mL) to an equimolar solution of $[Fe(bpca)_2]\cdot H_2O$ in nitromethane (2 mL). After 30 min of stirring at room temperature, the solution was left undisturbed in a desiccator. Well formed brown orange crystals resulted in several days. Compound **2** was obtained in a similar manner using a methanolic solution of $Gd(NO_3)_3\cdot 6H_2O$ (0.05 mmol) in methanol (2 mL) added to an equimolar solution of $[Fe(bpca)_2]NO_3$ in nitromethane (2 mL). Red orange block-shaped crystals suitable for single-crystal X-ray diffraction were obtained in several days. Crystals were used for X-ray and magnetic measurements.

Elemental analysis for $C_{26}H_{24}FeGdN_{11}O_{18}$ (**1**). Calcd (%): C, 31.49; H, 2.44; N, 15.54. Found (%): C, 31.63; H, 2.54; N, 14.95. Yield 63%. IR data (KBr, cm^{-1}): 3095(m), 1662(sh), 1645(s), 1597(m), 1554(m), 1535(m), 1506(m), 1371(s), 1302(m), 1275(m), 1038(w), 827(w), 765(m), 717(m), 653(w), 570(w), 520(m). Elemental analysis for $C_{29}H_{31}FeGdN_{14}O_{25}$ (**2**). Calcd (%): C, 29.28; H, 2.71; N, 16.48. Found (%): C, 29.56; H, 2.60; N, 16.32. Yield 48%. IR data (KBr, cm^{-1}): 1718(s), 1603(m), 1554(m), 1479(s), 1360(s), 1307(s), 1155(w), 1093(w), 1059(w), 1028(s), 810(w), 762(s), 744(m), 704(m), 656(w), 629(w), 517(w), 501(w).

2.3. Crystal Structure Determinations. The crystal data and details on the data collection and refinement for complexes **1** and **2** are summarized in Table S1 (Supporting Information). The crystal data for complexes **1** and **2** were collected using a Bruker SMART 1000 CCD-based diffractometer operating at 200 K. Intensities were collected with graphite monochromatized Mo Kα radiation (λ = 0.71073 Å) operating at 50 kV and 30 mA, using the $\omega/2\theta$ scan technique. The refinement method employed was full-matrix least-squares on F^2. The data integration and reduction were undertaken with SAINT and XPREP.[20] The intensity data were empirically corrected for absorption using the program SADABS.[21] The structures were solved using the Bruker SHELXTL software[22] by direct methods and refined by full-matrix least-squares methods on F^2. All non-hydrogen atoms were refined anisotropically, except in the case of crystallization solvents with some thermal disorder. Hydrogen atoms were included in calculated positions and refined in the riding mode.

Crystal data (**1**): $C_{26}H_{22}FeGdN_{11}O_{18}$, M = 989.65, T = 200 K, monoclinic, space group $P2_1/c$, a = 9.856(3) Å, b = 20.060(2) Å, c = 18.2973(16) Å, β = 100.457(4)°, V = 3526.5(7) Å^3, Z = 4, final R values are R_1 = 0.0678, wR_2 = 0.1568 for reflections with $I > 2\sigma(I)$ and R_1= 0.0977, wR_2 = 0.1722 for all data.

Crystal data (**2**): $C_{29}H_{31}FeGdN_{14}O_{25}$, M = 1189.74, T = K, triclinic, space group $P\bar{1}$, a = 11.164(3) Å, b = 13.617(4) Å, c = 15.816(5) Å, α = 103.315(6)°, β = 92.744(6)°, γ = 109.824(6)°, V = 2180.12 Å^3, Z = 2, final R values are R_1 = 0.0594, wR_2 = 0.1456 for reflections with $I > 2\sigma(I)$ and R_1 = 0.0726, wR_2 = 0.1528 for all data.

2.4. Physical Measurements. Fourier transform infrared spectroscopy was performed using a JASCO FT/IR-4200 instrument with KBr pellets in the 400−4000 cm^{-1} region (w, weak; m, middle strong; s, strong).

Magnetic measurements were carried out on a Quantum Design SQUID MPMS 5S magnetometer on polycrystalline samples, in a 0.1 T field over the temperature range 1.8−300 K.

dx.doi.org/10.1021/ic1023289 | Inorg. Chem. 2012, 51, 40−50

For magnetization measurements, the sample was restrained in eicosane to prevent torquing. Diamagnetic correction for each sample was determined using Pascal's constants. The ac magnetic susceptibility measurements were performed using a 0.3 mT magnetic field oscillating at 100−1000 Hz.

2.5. Ab Initio Calculations. The CASSCF (Complete Active Space Self Consistent Field) calculations and the subsequent *ab initio* Spin Orbit (SO) treatments were performed with the GAMESS program.[23] We used an SBKJC[24] effective core potential and basis set for lanthanide Gd, the 6-311G* basis set for the Fe, N, and O atoms, and 6-31G for the C and H skeleton.

3. RESULTS AND DISCUSSION

3.1. Crystal Structure Description. Compound **1**, $[Fe_{LS}^{II}(\mu\text{-bpca})_2Gd(NO_3)_2(H_2O)]NO_3{\cdot}2CH_3NO_2$, crystallizes in a monoclinic system, space group $P2_1/c$. Compound **2**, $[Fe_{LS}^{III}(bpca)(\mu\text{-bpca})Gd(NO_3)_4]{\cdot}4CH_3NO_2{\cdot}CH_3OH$, is triclinic, with the $P\bar{1}$ space group. Figure 1 shows the molecular units of compounds **1** and **2**, while Figure 2 shows a sequence of the chain structure of compound **1**. Selected bond lengths and angles are given in Table S2 in the Supporting Information.

In both systems, the anionic $bpca^-$ ligand acts as tridentate nitrogen donor toward the d ion (Fe(II) in compound **1** and Fe(III) in **2**). The iron centers are in both cases coordinated by six nitrogen donor atoms, in compressed octahedron geometries. The longer equatorial bonds are established with pyridine moieties (on average, 1.95 Å in compound **1** and 1.97 Å in compound **2**), with the axial ones being realized with the deprotonated amine nitrogen (on average, about 1.91 Å in both compounds). The formal negative charge enhances the coordination power of this type of donors. The axis of averaged compression in compound **2** is, in fact, unsymmetrical with respect to individual Fe(III)−N bond lengths: 1.95 Å for the central N donor of the ligand that participates in the bridge with Gd(III) and 1.89 Å for the opposite ligand. In compound **1**, where both ligands are acting as d−f bridges, the Fe−N bonds on the averagely short axis are closer to each other: 1.91 Å and 1.92 Å.

The carbonyl groups of the $bpca^-$ ligand afford the bridging of the f ion, with the whole $[Fe(bpca)_2]^q$ units (q = 0 for Fe^{II} and q = 1 for Fe^{III}) acting as complex ligands toward Gd(III). In compound **1**, Gd(III) is coordinated by two $[Fe_{LS}^{II}(bpca)_2]$ neutral units, two chelating nitrate ions, and one water molecule. The total coordination number is nine. The mean axes of the two coordinating diketonate fragments form an open angle (*ca.* 130°). Their chelating planes are approximately perpendicular to each other. This mutual placement creates the zigzag pattern of the chain. The two nitrate ion chelates are in a *cis* arrangement, with an approximate 90° angle between their mean coordination axes. The NO_3^- planes are also perpendicular to each other. One nitrate counterion is placed outside the chain, noncoordinated.

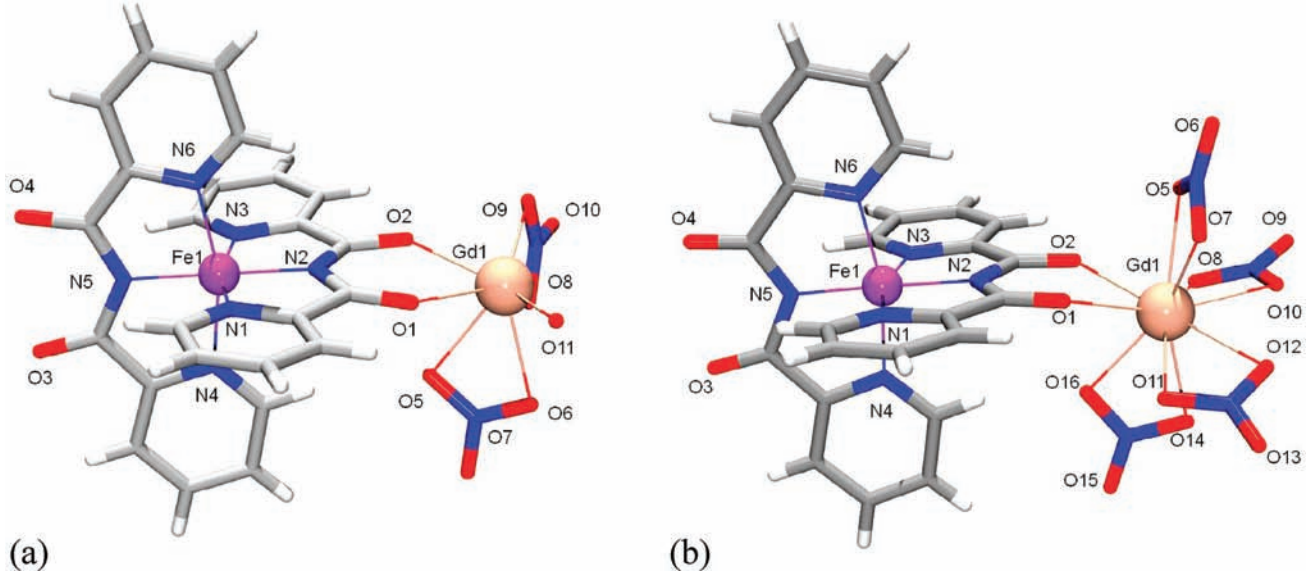

Figure 1. (a) Molecular unit, $[Fe_{LS}^{II}(\mu\text{-bpca})_2Gd(NO_3)_2(H_2O)]NO_3$, for compound **1** and (b) the dinuclear molecule $[Fe_{LS}^{III}(bpca)(\mu\text{-bpca})Gd(NO_3)_4]$ of compound **2** with the atom numbering scheme. Solvent molecules and the counter NO_3^- groups are omitted for clarity. Note that in part a the coordination of the Gd(III) site appears incomplete because of the eliminated continuation of the chain of compound **1**.

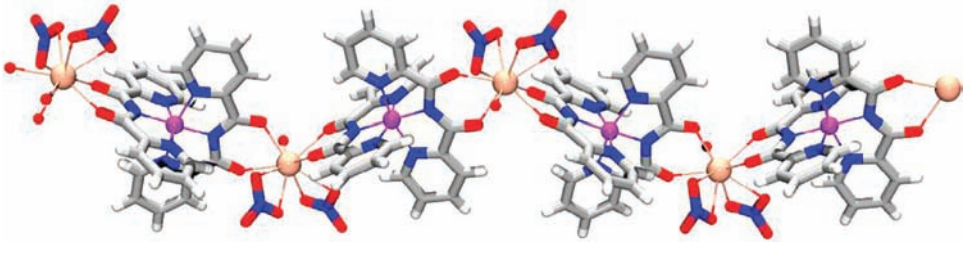

Figure 2. Sequence of the zigzag structure of compound **1**, $[Fe_{LS}^{III}(\mu\text{-bpca})_2Gd(NO_3)_2(H_2O)]NO_3{\cdot}2CH_3NO_2$.

dx.doi.org/10.1021/ic1023289 | *Inorg. Chem.* 2012, 51, 40−50

Apparently, the two complex $[Fe_{LS}^{II}(bpca)_2]$ ligands around the lanthanide ion are too bulky to allow the entry of the third nitrate in the coordination sphere, permitting only the smaller *aqua* ligand. The competition between nitrate and the complex ligand leads to a different structure in the case of compound **2**. The difference is made by the total charge of the complex ligand, which is positive for **2**, $[Fe_{LS}^{III}(bpca)_2]^+$. The total charge of the d complex and f cations is compensated by four nitrate ions, all of them being accommodated around the Gd(III) site. The ten-coordination number of the Gd(III) can be approximately described as a gyro-elongated square bipyramid.

3.2. Magnetic Properties. Figure 3 shows the χT vs T magnetic data for compounds **1** and **2**, limited to the interesting

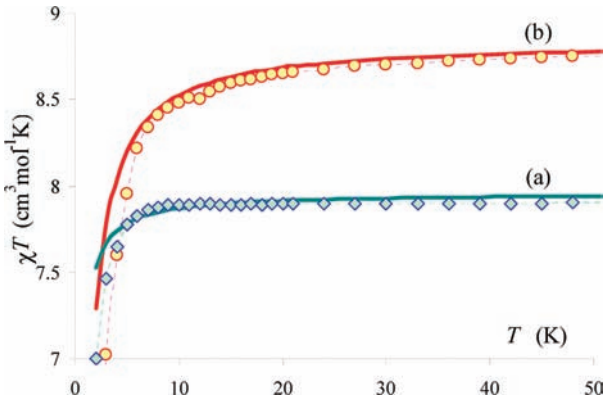

Figure 3. χT vs T experimental data (symbols and dashed lines) and theoretical curves (solid lines) for compound **1** (a) and compound **2** (b). The continuous lines are not parametric fits but correspond to the results obtained by introducing in the spin Hamiltonian models the parameters obtained directly from *ab initio* simulations. The only free parameters are g = 2.01 for compound **1** and g = 2.07 for **2**, adjusted to match the high temperature χT plateaus.

temperature interval 0−50 K. At a first glance, the pattern of both curves suggests antiferomangnetic-like behavior. Nevertheless, the situation deserves a detailed analysis. For compound **1**, the d site is nonmagnetic, Fe(II) is low-spin, and the distance between the Gd(III) ions is large, 11.3 Å. Therefore, it is unlikely to have a significant long-range superexchange coupling between the f ions over the Fe(II) complex bridges. It remains then to assume that the local ZFS is, probably, the effect determining the behavior of compound **1**. For **2**, the antiferomagnetic coupling is feasible, since the bpca$^-$ bridge may be a mediator of the d−f interaction. In this case, the question is how the local magnetic anisotropy and the intercenter exchange interaction are competing in the magnetic behavior of compound **2**. The fact that the ZFS and exchange effects are interplayed for compound **2** is suggested by the dynamic behavior revealed by the *ac* susceptibility measurements (Figure 4). The overview of the experimental data reflects complex effects, in spite of the relative simplicity with which the Gd(III) systems are usually conceived. The χT curves show, in fact, too few details to allow the salient determination of the needed parameters (e.g., for the system **2**, the J_{Gd-Fe} coupling altogether with D and E amounts for the ZFS on Gd(III)). The relatively rich data from the *ac* magnetic susceptibility measurements cannot be used for fitting with usual Heisenberg, ZFS, and Zeeman Hamiltonians. These models do not include the details related with spin dynamics and mechanisms of relaxation comprised in the experimental records.

For clarifying the parametric uncertainties, we also used *ab initio* methods. These procedures are presumably able to account for the relative magnitude of parameters and their range, in semiquantitative respects. In our case, the *ab initio* treatments yielded parameters that were inserted in the phenomenological spin Hamiltonians, leading to a reasonable match to the experimental data (see the next section and the Supporting Information). Apart from the small deviations below 5 K of the calculated curve from the experimental data, the *ab initio* approach succeeded in reproducing the major features of the χT curves (the position and the mean curvature of the region where the raising χT line bends to approach the plateau values).

Note that we do not perform a fit but directly use the *ab initio* parameters to mimic the magnetic susceptibility. For compound **1**, the computed ZFS parameters are D = 0.063 cm^{-1} and $|E|$ = 0.005 cm^{-1}. For compound **2**, the computed ZFS parameters are D = 0.047 cm^{-1} and $|E|$ = 0.004 cm^{-1}, while the exchange parameter is J_{GdFe} = −0.199 cm^{-1} (see the section 3.5), taken in the $\hat{H}_{exch} = -2J_{GdFe}\hat{S}_{Gd}\cdot\hat{S}_{Fe}$ convention of the spin coupling Hamiltonian. By chance of a good match, we can confine to using this value directly in the simulation of susceptibility of compound **2**. The E parameter is reported as a module, since the $\pm|E|$ values determine the same magnetic properties, with the switch of the sign being related to a conventional permutation of the x and y axes (by rotation around z, as visible in Figure S3 of the Supporting Information).

It is important to note certain details from tackling the magnetic susceptibility in the general circumstance of ZFS with $D \neq 0$ and $E \neq 0$. In the general case, with D and E active parameters, the S_z projections are no longer good quantum numbers. Then, the magnetic susceptibility cannot be rendered in the customary form, as the statistics of the S_z^2 amounts, over the spin states and their components, weighted with Boltzmann

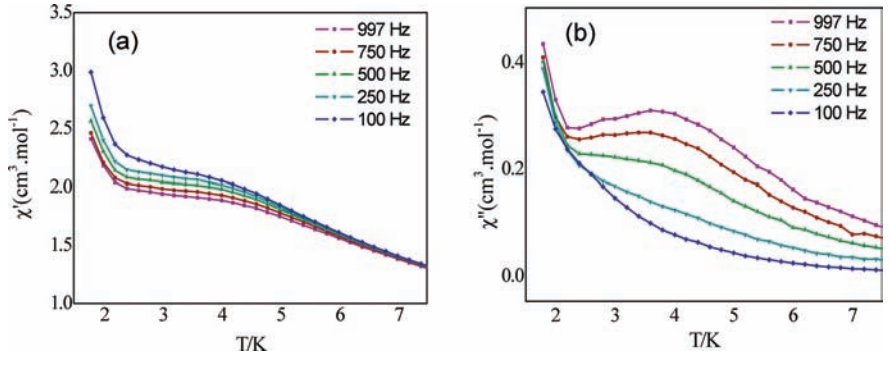

Figure 4. In-phase (a) and out-of-phase (b) magnetic susceptibility for compound **2**.

dx.doi.org/10.1021/ic1023289 | *Inorg. Chem.* 2012, 51, 40−50

factors for the corresponding spin Hamiltonian energies. Instead of using the simplest versions of the van Vleck formulas, based on the S_z (or M_s) indexing and summations, it is necessary to work here with equations derived with the help of the partition function Z, as expressed in the 1.3.1−1.3.7 formulas from page 5 in Kahn's book.[25] Because of the anisotropy induced by ZFS, the magnetization and susceptibilities must be taken as statistics over all space directions, assuming that the sample contains randomly oriented species. Thus, we treated the susceptibility with the following master formula:

$$\bar{\chi} = N_A k_B T \frac{1}{4\pi} \int_{\theta=0}^{\theta=\pi} \int_{\varphi=0}^{\varphi=2\pi} \left(\frac{d^2}{dB^2} \ln(Z(\theta, \varphi, B)) \right) \sin(\theta)\, d\theta\, d\varphi \quad (1)$$

where N_A and k_B are the Avogadro and Boltzmann constants and Z is the state function, i.e. the sum of Boltzmann factors for all the energies. This includes all the dependencies related to the spin Hamiltonian (ZFS and Heisenberg parameters) as well as the Zeeman dependence on the field B and its orientation, given in terms of the θ and φ polar angles. We performed the integration required by the averaging of the anisotropic susceptibility in a numerical manner, over a grid of 24 points for the θ coordinate and 48 points in the φ scan. The $\theta-\varphi$ mesh is similar to the partition of the globe by parallel and meridian lines, respectively. The derivatives of the partition function, Z, as well as those of the energies were taken numerically, by small dB = 0.001 T perturbations.

3.3. Phenomenology of Zero Field Splitting on Gd(III) Sites. We will present here aspects related with the general ZFS on the f^7 configuration. In spite of the fact that these are generalities, it is important to have them included in the discussion, because the possibility of the anisotropy on Gd(III) is often overlooked, as a consequence of its relatively small magnitude. The single ion anisotropy effects for Gd(III) are described by the ZFS operator:[25]

$$\hat{H}_{ZFS} = D\left(S_z^2 - \frac{1}{3}S(S+1)\right) + E(S_x^2 - S_y^2) \quad (2)$$

For the set of projections related with the $S = 7/2$ ground state, the solutions of the above Hamiltonian are resulting always in degenerate pairs, irrespective of the D and E values. This is because the full 8 × 8 matrix of the spin octet is factorized in two equivalent 4 × 4 blocks, as follows:

$$\begin{array}{cc} & \begin{matrix} -7/2 & -3/2 & +1/2 & +5/2 \end{matrix} \\ & \begin{matrix} +7/2 & +3/2 & -1/2 & -5/2 \end{matrix} \\ \begin{matrix} -7/2 & +7/2 \\ -3/2 & +3/2 \\ +1/2 & -1/2 \\ +5/2 & -5/2 \end{matrix} & \begin{pmatrix} 7D & \sqrt{21}E & 0 & 0 \\ \sqrt{21}E & -3D & 2\sqrt{15}E & 0 \\ 0 & 2\sqrt{15}E & -5D & 3\sqrt{5}E \\ 0 & 0 & 3\sqrt{5}E & D \end{pmatrix} \end{array} \quad (3)$$

The states interconnected in a block are either the {+7/2, +3/2, −1/2, −5/2} set or the {−7/2, −3/2, +1/2, +5/2} conjugated series, as figured on the row and column entries of the matrix given in eq 3. The matrix has this structure because the $E(S_x^2 - S_y^2)$ component of eq 2 interconnects, as nondiagonal elements, the spin projections with $\Delta S_z = \pm 2$.

The addition of the Zeeman Hamiltonian, for the interaction with the external magnetic field, further interconnects the elements satisfying the $\Delta S_z = \pm 1$ relationship. In this way, the two separate blocks are merged via the interaction of the $S_z = \pm 1/2$ elements, by a term related to the projection of the field in the xy plane. When the field is confined along the z axis, the two blocks remain yet independent. We point out that, even though the solutions of the ZFS Hamiltonian are degenerate, this does not simply originate from the DS_z^2 term acting on the $\pm S_z$ projections, being in turn related to the discussed symmetry of the equations. Since most often the lanthanide ions are placed in the asymmetric environments resulting from high coordination numbers, achieved with several different ligands, there is no reason to discard the E-type ZFS term. Figure 5 shows the pattern of the ZFS states as a function of the E vs D parametric ratio.

We will not detail here the Zeeman−Landé matrix elements, confining to a descriptive note that the terms related with the field along the z axis are contained as $-g\mu_B S_z B_z$ quantities along the diagonal of the matrices given in eq 3. The field along the x and y axes is equated in the nondiagonal elements between the basis components with a $\Delta S_z = \pm 1$ relation. As mentioned before, the Zeeman Hamiltonian interconnects in this way the two independent ZFS block matrices. A suggestive representation of the magnetic anisotropy on the f^7 ion is obtained considering the polar diagrams of the $|d\varepsilon_i/dB|$ derivatives for each i state of the $S = 7/2$ multiplet (see section A2 and Figure S3 of the Supporting Information). The first derivative has a magnetization-alike meaning, and taken as the polar diagram

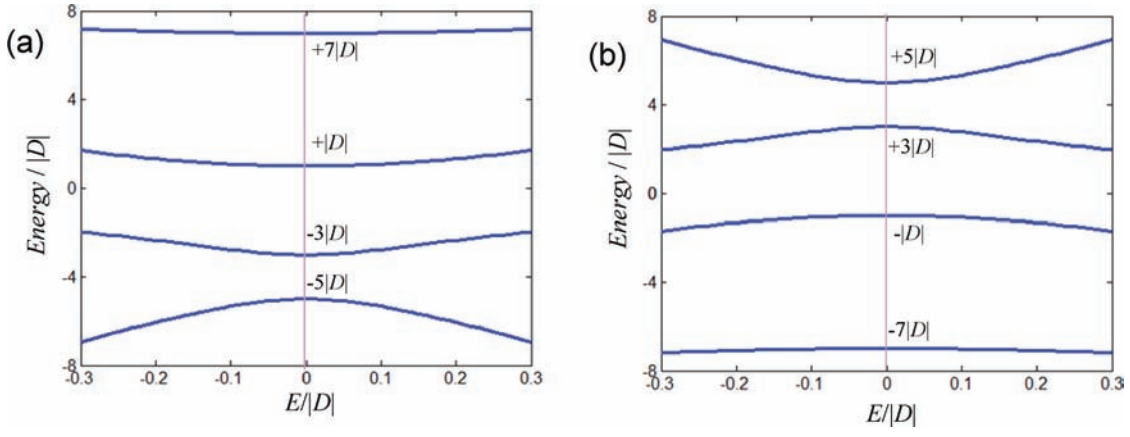

Figure 5. Pattern of the zero field splitting (ZFS) states in Gd(III) as a function of the $E/|D|$ ratio of the ZFS generic eq 1: (a) the $D > 0$ case; (b) the $D < 0$ case. The energy is presented also in $|D|$ relative units. Each line corresponds to a degenerate couple of levels, as described in eq 3. The E term leads to energy spectra different from the quadratic spacing determined by the D-only term.

dx.doi.org/10.1021/ic1023289 | Inorg. Chem. 2012, 51, 40−50

for a given state, it shows the response of the given level to the field perturbations from directions scanned in the 3D manner. The distance from the center to a surface point (measured along a given direction) amounts to the derivative of the energy with respect to the field, $|d\varepsilon_i/dB|$, obtained when the field was infinitesimally applied along that line. To get the derivative, we use the equations obtained by adding the Zeeman–Landé terms, $-g\mu_B\vec{S}\cdot\vec{B}$, of the interaction of the spin magnetic moments with the external magnetic field, $\vec{B}$, to the ZFS Hamiltonian from eq 3. The surfaces depicted in Figure S3 of the Supporting Information show an illustrative synopsis of the magnetic anisotropy associated with the ZFS of the f^7 configuration. For the isotropic case ($D = 0$, $E = 0$), the discussed polar diagrams are spheres with the $g\mu_B|S_z|$ radius. For the $D \neq 0$ and $E = 0$ case, magnetic anisotropy appears, with the corresponding surfaces having a two-lobe aspect. The maximal extension of the lobes is $g\mu_B|S_z|$, along the z axis. For the general case with $D \neq 0$ and $E \neq 0$, the S_z projections are no longer good quantum numbers, with the magnetization-alike polar representations of $|d\varepsilon_i/dB|$ being suggestive and alternative descriptors for the magnetic anisotropy of the given "i" state.

Early studies devoted to spectroscopy and EPR of Gd(III) ion assigned the ZFS to the mixing of the ground spin octet and excited sextet states.[26] Thus, the eigenvector of a ZFS component consists more than 95% in the ^8S ground state and about 2–3% in the ^6P state, with much lesser contributions from higher levels such as ^6D, ^6F, and ^6G. Besides, the occurrence of non-null D and E parameters implies local distortions from cubic or axial (tetragonal or trigonal) symmetries, respectively. The ZFS in the half filled shell of the f^7 configuration is formally similar to the d^5 case,[27] where, with respect to octahedral symmetry labels, the driving effect is the mixing, by spin–orbit and local distortions, of the $^6A_{1g}$ ground state (related with the ^6S atomic term) with the $^4T_{1g}$ level (originating from the ^4G excited atomic multiplet). The smaller ligand field makes the ZFS on the f^7 shell weaker than those of the d^5 high spin case, in spite of the fact that the spin orbit parameters are larger for lanthanides. For the free ions, the first spectral gap is about 32000 cm^{-1} for both the ^8S–^6P couple of Gd(III) and the ^6S–^4G one of Fe(III).[28] The larger ligand field in Fe(III) complexes determines a significant split of the ^4G term and smaller gaps with respect to the ground state, e.g. on the order of 10000 cm^{-1} for the $^6A_{1g}$–$^4T_{1g}$ couple in the octahedral field.[27] In turn, in the Gd(III) complexes, the first excited states remain approximately at the same separations as in the free ion, showing a small mixing with the ground state, determining small absolute ZFS parameters. The balance of ligand field and spin orbit effects that determine the D and E magnitudes for the f^7 ions is a complicated issue, due to the intricacies of ligand field models for lanthanides.[29] In the next section we will circumvent this complexity with the help of *ab initio* calculations.

3.4. *Ab Initio* Treatment of the Weak Magnetic Anisotropy of Gd(III) Sites. As mentioned in the introductory part, the calculation of the lanthanide system implies particular procedures, with customized algorithms,[12,10] beyond the standard controls of the used computer code. Our procedure starts from a "handmade" initial wave function, obtained by merging the orbitals of the separate fragments: the free lanthanide ions and the surrounding ligands. The starting LCAO matrices are then block diagonal, with zero elements in block nondiagonal areas, i.e. for the indices corresponding to the mutual mixing of the fragments. This starting wave function is consistent with the physical reality that the lanthanide ions are rather weakly interacting with the environment, in the ionic bonding regime. The CASSCF(n, m) calculations, with n electrons in m orbitals, are set to represent properly the problem at hand. The multiconfiguration setting is CASSCF(7,7) for Gd(III) sites in mononuclear units. This corresponds to the full configuration interaction in the ground ($S = 7/2$) and excited ($S = 5/2$) spin states arising from the f^7 configuration. The CASSCF calculation was followed by an *ab inito* spin orbit (SO) procedure, incorporating the levels related with the ^8S, ^6P, ^6I, ^6D, ^6G, ^6F, and ^6H terms of the free ion (in total, 49 orbital states).

Because the ZFS is an effect localized on a given site, it is reasonable to consider models having only the immediate ligand environment, taking approximations and cutting the moieties related to the long-range effects. Thus, from the chain structure of compound **1**, we idealized the Gd(III) coordination as a mononuclear complex made of the immediate coordinating ligands, $[Gd(Hbpca)_2(NO_3)_3(H_2O)]^+$, and eliminating the d metal ions and further 1D linkages.

For compound **2**, the *ab initio* ZFS approach can be reasonably simplified by ignoring the spin terms due to the paramagnetic Fe(III). This was achieved by replacing the Fe(III) with the diamagnetic Co(III), considering the calculation on the $[Co^{III}(bpca)(\mu\text{-}bpca)Gd(NO_3)_4]$ model. In this way, we are focused on the problems related with the f shell of gadolinium(III) ion.

The ZFS can be extracted from the small spacing obtained for the eight lowest levels resulting from the full CASSCF-SO calculation (the full spectrum consists of 269 spin-orbital terms). The levels are obtained in degenerate pairs (see discussion from section 3.3). Thus, for compound **1**, the following series of doublets is produced: {0.000, 0.148, 0.394, 0.770} cm^{-1}. This set is fitted by the eigenvalues of matrices from eq 3 by taking the $D = 0.063$ cm^{-1} and $|E| = 0.005$ cm^{-1} parameters. As shown in the previous section, these parameters, introduced in formula 1 for the averaged anisotropic susceptibility, match, at once, the pattern of the experimental χT vs T curve for system **1**. In a similar manner, the CASSCF-SO calculation of the Gd(III) site in complex **2** (taking the Co(III) idealized congener) yielded the following levels: {0.000, 0.117, 0.306, 0.585} cm^{-1}, which are fitted with $D = 0.047$ cm^{-1} and $|E| = 0.004$ cm^{-1}.

A significant development here is the characterization of anisotropy, drawing the polar surfaces of $|d\varepsilon_i/dB|$ functions for each state relevant for the ZFS spectrum. This is realized by handling the data contained in the black box of the CASSCF-SO *ab initio* spin–orbit calculations. Particularly, the extraction of the matrix elements and expectation values of the $\hat{L}_x$, $\hat{L}_y$, and $\hat{L}_z$ operators, which, altogether with the knowledge of spin-type Zeeman terms, based on the $\hat{S}_x$, $\hat{S}_y$, and $\hat{S}$ operators, affords the implementation of the field dependence in the CASSCF-SO *ab initio* matrices (using the specific $g_L = 1$ and $g_S = 2.0023$ Landé factors). Taking the numerical derivatives as the corresponding response functions of the system to a magnetic field, the magnetization surfaces are obtained in the full *ab initio* context, for correspondingly selected states. Since the macroscopic magnetization can be presented as a statistic over the $-d\varepsilon_i/dB$ amounts, weighted with corresponding Boltzmann factors,[25] the $-d\varepsilon_i/dB$ functions can be conventionally called state-specific magnetizations, as it is reasonable to consider the macroscopic results originating from a microscopic nature with a similar denomination. The polar representations of such state specific quantities are very illustrative for discussing the magnetic anisotropy as a function of the specific spectrum of states.

dx.doi.org/10.1021/ic1023289 | Inorg. Chem. 2012, 51, 40–50

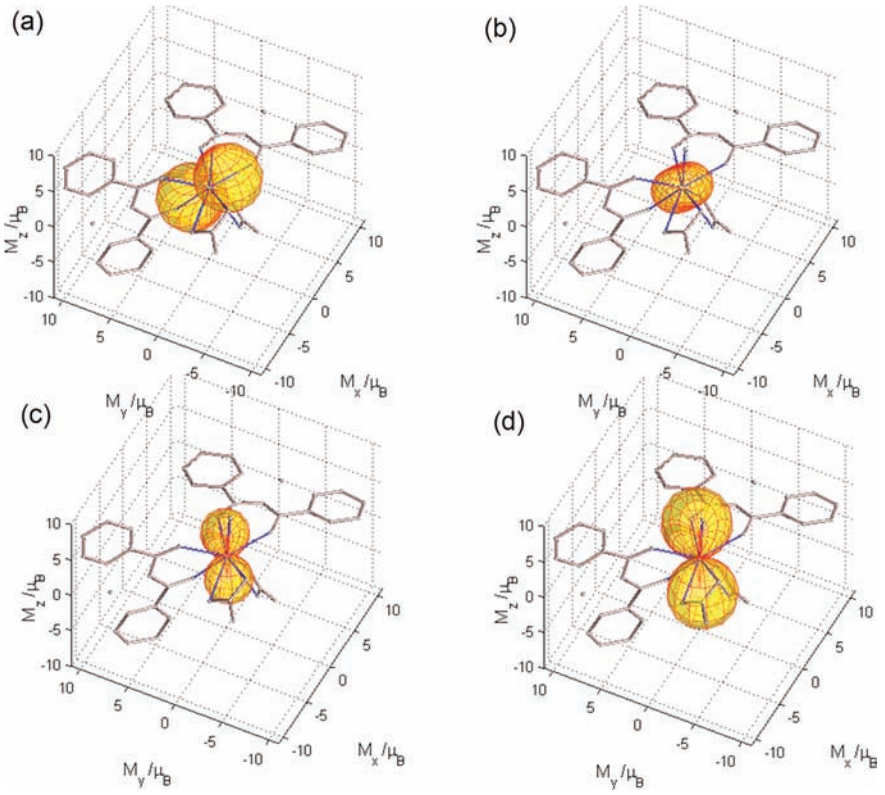

Figure 6. Polar representation of the |dε/dB| field derivatives (defined as state-specific magnetizations) obtained by full *ab initio* procedures and for the lowest pair of degenerate states of the Gd(III) site in compound **1.** Panels a−d correspond to degenerate pairs of anisotropic states with energies in the order a < b < c < d. The scale of the drawn molecular skeleton is arbitrary. The units for the M_x, M_y, and M_z axes are Bohr magnetons (μ_B). Each surface is encapsulated in a box with axes from $-10\mu_B$ to $+10\mu_B$, in all the *x*, *y*, *z* directions.

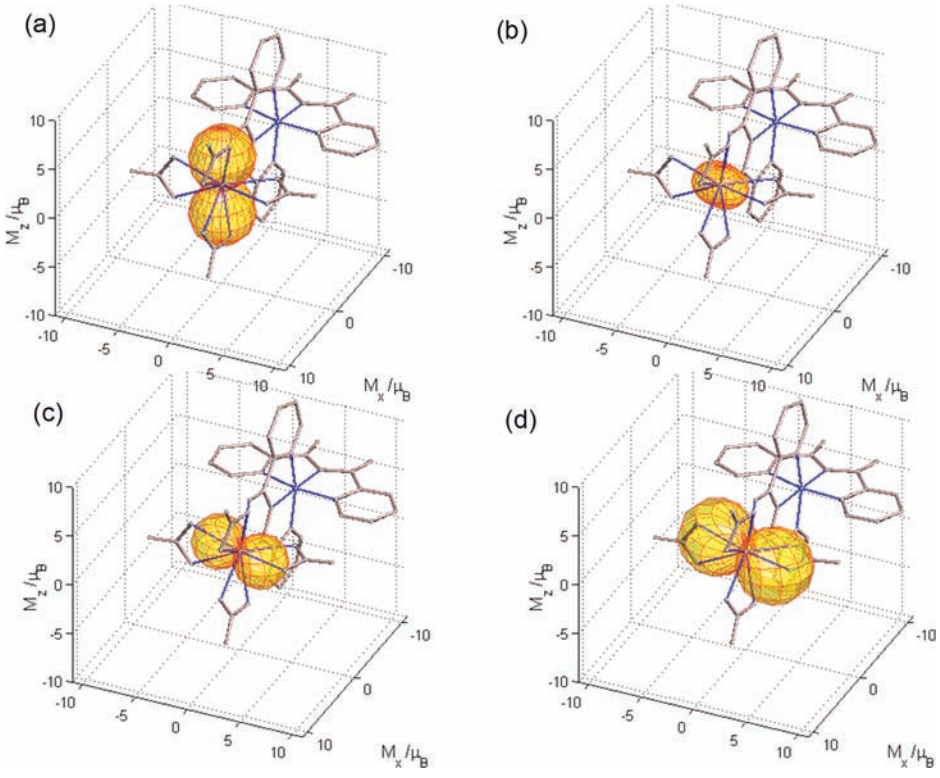

Figure 7. Polar representation of the |dε/dB| field derivatives (defined as state-specific magnetizations) obtained by full *ab initio* procedures, for the lowest pair of degenerate states of the Gd(III) site in compound **2**. Panels a−d correspond to degenerate pairs of anisotropic states with energies in the order a < b < c < d. The meaning of the representations is as explained in Figure 6.

dx.doi.org/10.1021/ic1023289 | *Inorg. Chem.* 2012, 51, 40−50

The results for the Gd(III) coordination spheres in **1** and **2** are presented in Figures 6 and 7, respectively. One observes that the patterns obtained for the polar diagrams in both **1** and **2** are similar to those outlined in Figure S3 of the Supporting Information.

Besides, replacing the above-mentioned *ab initio* resulted *D* and *E* parameters in the simplified model related to eq 3, i.e. the treatment related with Figure S3 of the Supporting Information, one obtained patterns closely similar to those from Figures 6 and 7. One must point out that, while the shapes in Figure S3 are obtained as response functions from phenomenological 8 × 8 Hamiltonian matrices, the results for real systems in Figures 6 and 7 are taken as the derivatives with the magnetic field from the 296 × 296 matrices, related with the applied CASCCF-SO calculations. The fact that the patterns of the small model and the full calculations coincide certifies the correctness of our nonroutine handling of the *ab initio* data.

A nontrivial result is the orientation of the magnetization lobes with respect to the molecular frames (Figures 6 and 7). The simplified frame of 8 × 8 discussed for eq 3 implies arbitrary sets of axes, while the full information contained in the 296 × 296 matrices enables the determination of effective magnetic anisotropy with respect to the molecular frame. These lobes identify the directions where the given state shows the highest sensitivity to magnetic field perturbations. The relative amplitudes of the lobes give information about the magnetic moment contained in a certain space direction, for the selected state. For compound **1**, the maximal lobe (with an extension of about $6.9\mu_B$, Figure 6d) is oriented approximately along a dihedral angle traced between the coordination axes of the two nitrate ligands. A lobe with comparable size ($6.6\mu_B$, in Figure 6a) is oriented along the axis of the *aqua* ligand. Smaller lobes, with $3.4\mu_B$ and $4.6\mu_B$ (Figure 6b and c) have the same axes as the respective 6a and 6d two-lobe surfaces. The maximal lobes define the easy magnetization axes. In this case, the pattern is similar to those revealed in the parametric experiments outlined above (see the discussion devoted to the cases from Figures S3.c and S3.d in the Supporting Information). The molecular unit of **2** is somewhat close to the C_s point group, in spite of the fact that this symmetry is not exact. The quasi-symmetry plane is parallel to the floor of the encapsulated coordinate insets from Figure 7. The state-specific magnetization lobes are oriented either perpendicularly or parallel to this approximate symmetry element (Figure 7).

3.5. Mechanism of Antiferromagnetic Coupling in d−f Complexes. In this section we will outline a mechanism for the antiferromagnetic case of d−f coupling. In the first instance, it can be considered as a qualitative heuristic proposal, aiming to counterpoint the relatively well-known situation of d−f ferromagnetism.[12−14] The ferromagnetic mechanism was discussed on Cu(II)−Gd(III) prototypic dinuclears,[12,13d] but it can be considered as a general scheme for d−f systems, because the implied reasons are valid for many conceivable structures with various transition metal and lanthanide ions (i.e., delocalization of the spin from singly occupied 3d-type AOs of transition metals, via bridges, toward the virtual 5d AOs of the lanthanide). The open question is, then, which is the mechanism explaining the complementary situations of d−f antiferromagnetism.[30] We propose here a scheme inspired by orbital particularities of compound **2**, but it can be conceived as more generally valid, being based on overlap symmetry and topological reasons. In the following we will denote by M the transition metal complex unit and by Ln the lanthanide ion.

In qualitative respects, the mechanism is suggested in Scheme 1 as due to a situation in which the unpaired 3d electrons do not find a convenient delocalization channel over the bridging ligand while, in turn, the delocalization is possible for a doubly occupied 3d component. This generic situation differs from those assigned to the ferromagnetic mechanism, where the delocalization 3d(M)-bridge-5d(Ln) is assumed to be the leading feature (e.g., realizable when the M and Ln ions touch the same bridging atom). In our case, the 3d(M)−4f(Ln) and 3d(M)−5d(Ln) interactions occur over a polyatomic bridge, with the delocalization being controlled by its topological factors. Thus, the orbitals in the t_{2g}^5-type set on the Fe(III) can be labeled, taking as reference the plane of the bridging moiety, as follows: $\pi_\parallel$ for the component contained in the ligand plane, $\pi_\perp$ for those perpendicular to the bridge and pointing two lobes along it (toward the Gd site), and δ for the component showing the 4 lobes in a plane perpendicular to the Fe−Gd axis (see notations in Scheme 1).

Scheme 1. Mechanism Proposed for the d−f Antiferromagnetism Observed in Compound 2[a]

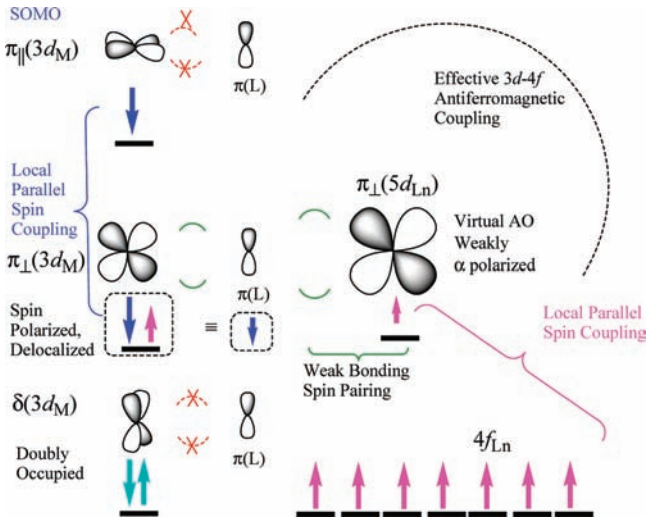

[a]The balance of spin polarization and delocalization effects can be conceived as general for other situations, characterized by subsets containing closely spaced doubly and singly occupied 3d orbitals. The key feature is having delocalization banned for 3d orbitals carrying unpaired electrons but allowed for doubly occupied orbitals. In this case, the delocalization can occur in a polarized manner.

Among the d-type components of the t_{2g} set, only the $\pi_\perp$ one is capable of interaction with the delocalized π system of the bridging aromatic ligand and furthermore with the 5d AOs on the lanthanide. The $\pi_\parallel$ and δ components are not favorable for the delocalization over the ligand and, effectively, cannot communicate with the lanthanide site. A key feature suggested in Scheme 1 is a ligand field ordering placing the unpaired electron in an orbital not favorable for delocalization, e.g. $\pi_\parallel$, precluding the mechanism that leads to ferromagnetism. The scheme remains the same if the δ component is the highest one, but it turns to a ferromagnetic mechanism if the $\pi_\perp$ carries the unpaired electron.

There are simplistic reasons that support the $\delta(3d_M)$ as the lowest orbital in the t_{2g} ligand field split, while the $\pi_\parallel(3d_M)$ is the higher one. Thus, the $bpca^-$ ligand exerts anisotropic π perturbations, with the central amine nitrogen behaving most

dx.doi.org/10.1021/ic1023289 | Inorg. Chem. 2012, 51, 40−50

probably as donor, because it carries a formal negative charge, while the pyridine moieties are presumably π-acceptors.[31] The δ-type 3d AO overlaps only with pyridine components from both bpca$^-$ ligands (and has no interaction with the amine donors); the π-acceptor features of the interaction suggest that this orbital is the lowest in the ligand field splitting of the t_{2g} set. The $\pi_\perp$ ($3d_M$) interacts via proper π_{d-p} overlapping with the bridging ligand. In turn, the $\pi_\parallel(3d_M)$ interacts in the same way with the nonbridging one, with the reverse situation occurring because the two bpca$^-$ ligands are mutually perpendicular. A difference in the perturbation power of the two ligands can be found in the charge distribution on their diketonate moieties. A negative charge is formally smeared among the electronegative atoms of the diketonate: one amine nitrogen and two carbonyl oxygen atoms in each ligand. In the nonbridging ligand case, the positive charge of the transition metal body attracts more negative charge on the central nitrogen, which, in turn, causes a higher perturbation of the electrons in the $\pi_\parallel(3d_M)$ orbital, as compared to the $\pi_\perp(3d_M)$ one. Conversely, for the briding ligand, the negative charge is less polarized toward the M transition metal center, due to electrostatic competition exerted by the opposite Ln ion. The bridging ligand will exert, therefore, a lesser perturbation power toward the corresponding interacting orbital, $\pi_\perp(3d_M)$. The larger coordination power of the nonbridging bpca$^-$ ligand is also in line with the shorter Fe−N bond length discussed in the previous structural section.

Thus, for simplistic overlap and electrostatic reasons, the splitting of the t_{2g} set is suggested as $\delta < \pi_\perp < \pi_\parallel$. If we consider the bridging ligand in the *xz* plane, this order is equivalent to the $d_{xy} < d_{yz} < d_{xz}$ sequence. This sort of orbital scheme seems also supported by the *ab initio* reasons (see panel S4.a in Figure S4 of the Supporting Information). In fact, in the *ab initio* results, the higher and lower canonical orbitals assignable to the Fe(III) site look like a mutual mixing of the δ and $\pi_\parallel$ components, but this does not impinge upon the proposed heuristic mechanism, since both of these are nonfavorable to bridge delocalization effects, with the key of the mechanism staying in such a feature.

The premises of the proposed mechanism are as follows: (i) the delocalization of orbitals carrying unpaired electrons on the transition metal site (over the bridge, toward the lanthanide site) is disfavored by topological factors; (ii) the delocalization is possible for a doubly occupied component and occurs in a spin-polarized manner, i.e. creating a slight α vs β incremental spin density separation at the opposite ends of the complex, at the M and Ln sites; (iii) the local exchange effects lead to parallel alignment of spin densities from singly occupied MOs and residual spin components from polarization, on each M and Ln unit; (iv) because the main spin on a given moiety (M or Ln) holds parallel to those resulting from the polarization of the doubly occupied orbital, while the residual spin densities resulting from the polarized delocalization are mutually opposed, an overall antiferro coupling results.

The polarization invoked in the above (ii) line can be understood by the fact that the bonding established between the M and Ln units is, in fact, a weak covalence,[15] where the M complex uses an orbital delocalized over the 3d site and bridge, $d(\pi_\perp)-L(\pi)$, as donor interacting with the virtual 5d AOs, which acts as acceptor, on the lanthanide. In terms of valence bond concepts,[33] the covalent bonding, even a weaker long-range one, is an antiferro-like spin coupling. Conceived for a weak bonding and residual charge density displacement, this implies a spin polarization between the delocalized $d(\pi_\perp)-L(\pi)$ MO, at one side, and the 5d(Gd) ones, on the other part. At the same time, the spin polarization at a local site, either the Fe(III) or the Gd(III), enforces a parallel orientation of partial spin densities to the main spin density located in the singly occupied molecular orbital components (SOMOs) of the given ion. In this way, a chain of mutual relationships that leads to final antiferromagnetic coupling of the Gd(III) and Fe(III) sites is realized.

The role of spin polarization in the proposed mechanism is also suggested by an *ab initio* series of numeric experiments with successively enhanced active spaces. The CASSCF(12,10) calculation (i.e., 12 electrons in 10 orbitals), using an active space containing the t_{2g}^5 octahedral-type configuration on the iron(III) unit and the f^7 shell of gadolinium(III), yielded a very weak ferromagnetic coupling, $J_{GdFe} = 0.02$ cm^{-1}. An alternative numeric experiment, CASSCF(8,12), considering only the SOMO electrons from the 3d and 4f paramagnets and the empty orbitals resembling the 5d shell on Gd(III), also yielded a weak ferromagnetism, $J_{GdFe} = 0.03$ cm^{-1}. Therefore, neither the doubly occupied d-type MOs on Fe(III) nor the empty d virtuals on Gd(III), considered separately, lead to antiferromagnetism. In turn, this appears in the enhanced active space that includes both types of components, suggesting the role of delocalization−polarization route. Indeed, a multiconfiguration self-consistent field treatment (MCSCF) including the t_{2g}^5(Fe), f^7(Gd), and $5d^0$(Gd) sets, yielded a sizable antiferromagnetic coupling, with $J_{GdFe} = -0.199$ cm^{-1}, suggesting that the mutual interaction of doubly occupied, singly occupied, and empty orbitals is the key of antiferro manifestation. Since the fully CASSCF(12,15) was prohibitive in this case, the performed MCSCF used the ORMAS (occupation restricted multiple active spaces)[32] partition technique, defining three subspaces, namely the t_{2g}^5(Fe), f^7(Gd), and $5d^0$(Gd) sets, performing CASSCF inside each subspace and allowing single and double excitations among spaces. As noticed in advance, the $J_{GdFe} = -0.199$ cm^{-1} value, and the corresponding *D* and *E* parameters computed for compound **2**, retrieve quite closely the experimental magnetic susceptibility, without further fit (see Figure 3, curve b). We regard this result as a fortunate one, since we do not usually expect from a calculation to retrieve the experiment completely. However, we expect that the order of magnitude, the relative size of the parameters (exchange vs ZFS, *D* vs *E*), and their signs are well accounted for and that properly settled numerical experiments can reveal clues of the interaction mechanisms.

Otherwise, the calculations were performed in semiquantitative respects and should be regarded critically and as a matter of further challenge, because of certain drawbacks related with the limited quality of the basis sets. Namely, the 6-311G* basis set is unable to find the right high spin (HS) vs low spin (LS) balance on Fe(III), because of the overestimation of the two-electron Racah parameters.[34a] For instance, for the free Fe(III) ion, the CASSCF(5,5) calculations (i.e., an active space with five electrons in five orbitals) yield a spectrum fitted with the $B = 1320$ cm^{-1} and $C = 4938$ cm^{-1} Racah parameters, while the fit to experimental data[28a] is accomplished with $B = 1067$ cm^{-1} and $C = 4159$ cm^{-1} (see section A4 in the Supporting Information). The condition for reaching the LS state implies, in a rough approximation, a $10Dq$ ligand field splitting parameter larger than the $7.5B + 5C$ pairing energy, or $27.5B$ if we adopt the further approximation $C \sim 4B$[34b] (see section A5 in the Supporting Information).

dx.doi.org/10.1021/ic1023289 | *Inorg. Chem.* 2012, 51, 40−50

Due to overestimation of the one-center B and C integrals, the ground state of the Fe(III) unit in compound **2** is obtained in HS form, instead of the experimental LS configuration. At the same time, there is no experimental doubt that the $[Fe(bpca)_2]^+$ unit is in LS form, with the experimental plateau values of the χT being consistent with a spin-only $S = 1/2$ contribution from this unit. Besides, related[9] and isostructural[10] analogues of the present systems were characterized previously (e.g., by Mössbauer spectra), proving the LS configuration.

In our opinion, the *ab initio* calculations yield a good description of ligand field local effects and intercenter exchange interactions (i.e., $10Dq$ and J-type parameters), in spite of the certain flaws in the account of the one-center interelectron part. According to our preliminary investigation, the overestimation of the B and C integrals is due to a slightly shorter effective radius of the d shell, and this is a general characteristic of many basis sets, over all the transition metal atoms. This situation does not have drawbacks in most cases, except certain accidents in the HS−LS subtle balance, where the $10Dq$ and other ligand field parameters are accounted for well, but the systems expected in the LS state remain in HS form, because of the overestimated Racah parameters. Even relatively important for such one-site effects, this kind of slight shift of an effective d shell radius, δR, cannot affect largely the intercenter integrals computed at a given R interatomic spacing, since the power series terms that equate the specific differences, $(\delta R/R)^n$, become negligible. Therefore, we opine that the exchange coupling is reasonably described, in spite of a slight misfit in the one-site one-electron vs two-electron balance. If we confine the active space to the t_{2g}^5 set, where only a LS configuration is possible, in accordance with the experimental situation, one reaches a satisfying semiquantitative description of the exchange effects relative to this state.

The methodological issue related with the overestimation of Racah parameters deserves further attention, hopefully concretized with the obtainment of a series of basis sets of double- or triple-ζ quality with good retrieval of the free atom parameters. As chemists, our perspective is that the basis sets of moderate size afford a tractable and transparent use of computational chemistry as a complement to experiment, while the perfect reproduction of certain spectral features at the expense of very large basis sets and heavy calculation procedures is a separate theoretical deal and does not necessarily serve better the insight aims.

Another issue that deserves further detailed analysis is the possibility of an exchange anisotropy induced by the electronic configuration of the Fe(III) site.[35] At a first glance, there are reasons to ignore in our case such effects, related with the formal degeneracy expected in the ideal octahedral frame, where a $^2T_{2g}$ term is the lowest spin doublet. The $[Fe(bpca)_2]^+$ unit is, in fact, quite distant from the ideal octahedral frame, first by an axial compression, that formally brings the frame toward the D_{2d} symmetry, and then by the asymmetry caused by the d−f association, that reduces the possible maximal symmetry to C_s. The relatively significant differences between the two bpca$^-$ ligands are mentioned in the structure description. The CASSCF(12,10) calculation corresponding to an active space containing the t_{2g}^5 octahedral-type configuration on the iron(III) unit and the f^7 shell of gadolinium(III) showed that the sequence assignable to the t_{2g}^5 ligand field states presents a definite lift of degeneracy with levels at 0, 749.7, and 1264.5 cm^{-1}. Each of these three ligand field configurations implies a different J parameter, describing the further split resulting from exchange coupling with the Gd(III) center. The anisotropy of exchange would result from a perturbation mixing of state-sensitive J parameters, reflected in susceptibility, when the system is scanned with a magnetic field. However, the gaps in the order of several hundreds of reciprocal centimeters encountered due to the ligand field part cannot produce a large perturbation involvement of the exchange coupling from the next excited states. Or, if this effect is expected, it will be marked by variations at larger temperature in the χT vs T curves, because it will be causally due to effects implying interstate-gaps in the 10^2 cm^{-1} range. The effects occurring in the low temperature branch, as is the discussed case, are consistent with smaller scale effects, in the 10^{-1} cm^{-1} range, assignable to the f slight anisotropy and small d−f exchange. The ruling out of exchange anisotropy in this way is, however, a qualitative reasoning, and the possible implications of such effects may deserve further consideration. Useful details on the present level of *ab initio* modeling are given in the Supporting Information.

4. CONCLUSION

We reported the results of a combined experimental and theoretical study, which, in the synthetic part, exploited the capability of the bpca$^-$ ligand to form d−f compounds. We analyzed the magnetostructural features of a Fe(II)−Gd(III) chain (compound **1**) and a Fe(III)−Gd(III) dinuclear (compound **2**). These served as case studies for investigating, with advanced theoretical methods, the role of the ZFS as well as of the interplay between the magnetic anisotropy and the exchange coupling effects in the magnetochemistry of Gd(III) complexes. The compounds studied are best suited for this quest, because system **1** offers a case of very likely stand-alone ZFS, with the Fe(II) site being low spin and diamagnetic, while system **2** witnesses combined ZFS and exchange coupling. The latter is also structurally simple, allowing the advanced investigation with subsequent calculations and models.

We presented insight that challenges the customary view that the gadolinium ions have quite plain and simple isotropic magnetochemistry. Even though small, the ZFS effects play a significant role in the details of the magnetic behavior. The decryption of the ZFS effects on gadolinium has subsequent relevance, as it forms the ground for using Gd(III) complexes as contrasting agents in modern medical resonance devices.

We reported breakthroughs in the interpretation of small, but relevant, magnetic anisotropy of gadolinium complexes via *ab initio* state of the art procedures. A valuable result is the reported possibility to discriminate details of magnetic anisotropy, with respect to the molecular frame, from the orientation and magnitude of the polar representation of magnetization-alike surfaces for individual states, with compounds **1** and **2** serving as picturesque illustrations. An interesting finding was that the computed ZFS and exchange coupling constant describe well the experimental pattern of the magnetic susceptibility for both compounds **1** and **2**. Another outcome is a mechanism proposed for the antiferromagnetic coupling in d−f heterometallic complexes, taking compound **2** as a case study. This result complements the mechanism revealed in our previous analysis,[12] for the case of the d−f ferromagnetic effect. The prerequisite for such a mechanism is a ligand field scheme with relatively small orbital spacing (on the order of 10^2−10^3 cm^{-1}) between double and single occupied orbitals of the 3d metal ions, in order to facilitate the local polarization effects. The split of the octahedral t_{2g} set due to low symmetry in the range of a few hundred inverse centimeters is

dx.doi.org/10.1021/ic1023289 | Inorg. Chem. 2012, 51, 40−50

sufficiently large to remove the orbital magnetic components, but it is small enough to favor the mentioned spin polarization scheme. By contrast, the mechanism known for Cu−Gd ferromagnetism corresponds to the cases where polarization involving the inner doubly occupied d orbitals does not occur. There, the doubly occupied orbitals are, for ligand field reasons, well separated from the SOMO (on the order of 10^3−10^4 cm^{-1}) and therefore weakly interacting. The proposed mechanism covers the absence of previous hypotheses in the matter of antiferromagnetic d−f cases.

■ ASSOCIATED CONTENT

Supporting Information

Additional crystallographic data in cif format for compounds **1** and **2**; details of the phenomenological modeling of anisotropy and *ab initio* calculations. This material is available free of charge via the Internet at http://pubs.acs.org.

■ AUTHOR INFORMATION

Corresponding Author

*E-mail: M.F., marilena.cimpoesu@g.unibuc.ro; F.C., cfanica@yahoo.com.

■ ACKNOWLEDGMENTS

This work is supported from the research grants CNCS-UEFISCDI PCCE 9/2010, Romania.

■ REFERENCES

(1) (a) Ishikawa, N. *Funct. Phthalocyanine Mol. Mater., Struct. Bonding* **2010**, *135*, 211. (b) Sessoli, R.; Powell, A. K. *Coord. Chem. Rev.* **2009**, *253*, 2328−2341. (c) Andruh, M.; Costes, J. P.; Diaz, C.; Gao, S. *Inorg. Chem.* **2009**, *48*, 3342−3359.

(2) (a) Bünzli, J. C. G. *Chem. Rev.* **2010**, *110*, 2729−2755. (b) Eliseeva, S. V.; Bunzli, J. C. G. *Chem. Soc. Rev.* **2010**, *39*, 189−227.

(3) Ma, L. Q.; Lin, W. B. *Funct. Metal−Organic Frameworks: Gas Storage, Sep. Catal., Top. Catal.* **2010**, *293*, 175.

(4) Caravan, P.; Ellison, J. J.; McMurry, T. J.; Lauffer, R. B. *Chem. Rev.* **1999**, *99*, 2293−2352.

(5) Cotton, S. *Lanthanide and actinide chemistry*; John Wiley & Sons: New York, 2006.

(6) Tanase, S.; Reedijk, J. *Coord. Chem. Rev.* **2006**, *250*, 2501−2510.

(7) Costes, J.-P.; Garcia-Tojal, J.; Tuchagues, J.-P.; Vendier, L. *Eur. J. Inorg. Chem.* **2009**, 3801−3806.

(8) Benmelouka, M.; Van Tol, J.; Borel, A.; Port, M.; Helm, L.; Brunel, L. C.; Merbach, A. E. *J. Am. Chem. Soc.* **2006**, *128*, 7807−16.

(9) Kajiwara, T.; Nakano, M.; Kaneko, Y.; Takaishi, S.; Ito, T.; Yamashita, M.; Igashira-Kamiyama, A.; Noiri, H.; Ono, Y.; Kojima, N. *J. Am. Chem. Soc.* **2005**, *127*, 10150−10151.

(10) Ferbinteanu, M.; Kajiwara, T.; Choi, K.-Y.; Nojiri, H.; Nakamoto, A.; Kojima, N.; Cimpoesu, F.; Fujimura, Y.; Takaishi, S.; Yamashita, M. *J. Am. Chem. Soc.* **2006**, *128*, 9008−90009.

(11) (a) Ferbinteanu, M.; Kajiwara, T.; Cimpoesu, F.; Katagiri, K.; Yamashita, M. *Polyhedron* **2007**, *26*, 2069−2073. (b) Ferbinteanu, M.; Cimpoesu, F.; Kajiwara, T.; Yamashita, M. *Solid State Sci.* **2009**, *11*, 760−765.

(12) Paulovic, J.; Cimpoesu, F.; Ferbinteanu, M.; Hirao, K. *J. Am. Chem. Soc.* **2004**, *126*, 3321−3331.

(13) (a) Bencini, A.; Benelli, C.; Caneschi, A.; Dei, A.; Gatteschi, D. *Inorg. Chem.* **1986**, *25*, 572−575. (b) Figuerola, A.; Diaz, C.; Ribas, J.; Tangoulis, V.; Sangregorio, C.; Gatteschi, D.; Maestro, M.; Mahia, J. *Inorg. Chem.* **2003**, *42*, 5274−5281. (c) Kahn, M. L.; Sutter, J. P.; Golhen, S.; Guionneau, P.; Ouahab, L.; Kahn, O.; Chasseau, D. *J. Am. Chem. Soc.* **2000**, *122*, 3413−3421. (d) Costes, J.-P.; Dahan, F.; Dupuis, A.; Laurent, J.-P. *Inorg. Chem.* **1996**, *35*, 2400−2400. (e) Costes, J.-P.; Dahan, F.; Dupuis, A.; Laurent, J.-P. *Inorg. Chem.* **1997**, *36* (3429−3433), 4284−4286.

(14) (a) Benelli, C.; Gatteschi, D. *Chem. Rev.* **2002**, *102*, 2369−2387, and references therein. (b) Kahn, O. *Acc. Chem. Res.* **2000**, *33*, 647−657. (c) Sakamoto, M.; Manseki, K.; Okawa, H. *Coord. Chem. Rev.* **2001**, *379*, 219−221, and references therein.

(15) Ferbinteanu, M.; Zaharia, A.; Gîrţu, M. A.; Cimpoesu, F. *Cent. Eur. J. Chem.* **2010**, *8*, 519−529.

(16) Rajaraman, G.; Totti, F.; Bencini, A.; Caneschi, A.; Sessoli, R.; Gatteschi, D. *Dalton Trans.* **2009**, 3153−3161.

(17) (a) Swerts, B.; Chibotaru, L. F.; Lindh, R.; Seijo, L.; Barandiaran, B.; Clima, B.; Pierloot, K.; Hendrickx, M. F. A. *J. Chem. Theory Comput.* **2008**, *4*, 586−594. (b) Chibotaru, L. F.; Ungur, L.; Soncini. *Angew. Chem., Int. Ed.* **2008**, *47*, 4126−4129.

(18) Private discussion with L. F. Chibotaru and co-workers, during joint meetings and reports of the INTAS Grant 00-00565/2003-2005, devoted to lanthanide structure and magnetism, the frame in which our methodology for the d−f *ab initio* approach was initially developed.

(19) Wocadlo, S.; Massa, W.; Folgado, J.-V. *Inorg. Chim. Acta* **1993**, *207*, 199.

(20) SMART, SAINT, and XPREP, Area detector control and data integration and reduction software; Bruker Analytical X-ray Instruments Inc.: Madison, WI, 1995.

(21) Sheldrick, G. M. SADABS. Program for Empirical Absorption Correction of Area Detector Data; University of Göttingen: Germany, 1996.

(22) Sheldrick, G. M. *SHELXS-97*, A Program for Solving Crystal Structures and Crystal Structure Refinement; University of Göttingen: Göttingen, Germany, 1997.

(23) Schmidt, M. W.; Baldridge, K. K.; Boatz, J. A.; Elbert, S. T.; Gordon, M. S.; Jensen, J. H.; Koseki, S.; Matsunaga, N.; Nguyen, K. A.; Su, S. J.; Windus, T. L.; Dupuis, M.; Montgomery, J. A. *J. Comput. Chem.* **1993**, *14*, 1347−1363.

(24) (a) Day, P. N.; Jensen, J. H.; Gordon, M. S.; Webb, S. P.; Stevens, W. J.; Krauss, M.; Garmer, D.; Basch, H.; Cohen, D. *J. Chem. Phys.* **1996**, *105*, 1968−1986. (b) Jensen, J. H. *J. Chem. Phys.* **2001**, *114*, 8775−8783.

(25) Kahn, O. *Molecular Magnetism*; VCH Publishers: New York, 1993.

(26) (a) Wybourne, B. G. *Phys. Rev.* **1966**, *148*, 317−327. (b) Newman, D. J.; Urban., W. *Adv. Phys.* **1975**, *24*, 793−843.

(27) Gerloch, M.; Lewis, J.; Slade, R. C. *J. Chem. Soc. (A)* **1969**, 1422.

(28) (a) Moore, C. E. *Atomic Energy Levels as Derived from the Analysis of Optical Spectra—Chromium through Niobium*. In *Nat. Stand. Ref. Data Ser., NSRDS-NBS 35*, Vol. *II*; National Bureau of Standards: U.S., 1971. (b) Martin, W. C.; Zalubas, R.; Hagan, L. *Atomic Energy Levels—The Rare-Earth Elements*; In *Nat. Stand. Ref. Data Ser., NSRDS-NBS 60*; National Bureau of Standards, U.S., 1978.

(29) (a) Newman, D. J.; Ng, B. K. C. *Crystal Field Handbook*; Cambridge University Press: Cambridge, 2000. (b) Edvardsson, S.; Åberg, D. *Comput. Phys. Commun.* **2001**, *133*, 396−406.

(30) (a) Costes, J.-P.; Dahan, F.; Dupuis, A.; Laurent, J.-P. *Inorg. Chem.* **2000**, *39*, 169−173. (b) Costes, J.-P.; Dahan, F.; Dupuis, A. *Inorg. Chem.* **2000**, *39*, 5994−6000.

(31) (a) Lever, A. B. P. *Inorganic Electronic Spectroscopy*, 2nd ed.; Elsevier Publishing Co.: Amsterdam, 1984; p 52. (b) Solomon, E. I.; Lever, A. B. P. *Inorganic Electronic Structure and Spectroscopy*; Willey & Sons: New York, 1999; Vol. *I*, pp 22, 32.

(32) Ivanic, J. *J. Chem. Phys.* **2003**, *119* (9364−9376), 9377−9385.

(33) Cooper, D. L., Ed. *Valence Bond Theory*; Elsevier Science: Amsterdam, 2002.

(34) (a) Racah, G. *Phys. Rev.* **1942**, *62*, 438−462. (b) Tanabe, Y.; Sugano, S. *J. Phys. Soc. Jpn.* **1954**, *9*, 766−779.

(35) Atanasov, M.; Comba, P.; Daul, C. A. *Inorg. Chem.* **2008**, *47*, 2449−2463.